

# Learning Nonlinear Input-Output Maps with Dissipative Quantum Systems

Jiayin Chen and Hendra I. Nurdin\*

*School of Electrical Engineering and Telecommunications,  
The University of New South Wales (UNSW), Sydney NSW 2052, Australia*

## Abstract

In this paper, we develop a theory of learning nonlinear input-output maps with fading memory by dissipative quantum systems, as a quantum counterpart of the theory of approximating such maps using classical dynamical systems. The theory identifies the properties required for a class of dissipative quantum systems to be *universal*, in that any input-output map with fading memory can be approximated arbitrarily closely by an element of this class. We then introduce an example class of dissipative quantum systems that is provably universal. Numerical experiments illustrate that with a small number of qubits, this class can achieve comparable performance to classical learning schemes with a large number of tunable parameters. Further numerical analysis suggests that the exponentially increasing Hilbert space presents a potential resource for dissipative quantum systems to surpass classical learning schemes for input-output maps.

---

\* h.nurdin@unsw.edu.au (corresponding author)

## I. INTRODUCTION

We are in the midst of the noisy-intermediate quantum technology (NISQ) era [33], marked by noisy quantum computers consisting of roughly tens to hundreds of qubits. Currently there is a substantial interest in early applications of these machines that can accelerate the development of practical quantum computers, akin to how the humble hearing aid stimulated the development of integrated circuit (IC) technology [26]. NISQ quantum computing machines will not be equipped with quantum error correction and are thus incapable of performing continuous quantum computation.

Several research directions are being explored for NISQ-class machines. One direction is to demonstrate so-called “quantum supremacy”, in which NISQ machines can perform computational tasks that are demonstrably out of the reach of the most powerful digital supercomputers. The computational tasks include sampling problems such as boson sampling [1, 23], instantaneous quantum polynomial (IQP) computation [7, 23], and sampling from random quantum circuits [4]. Another direction is the development of variational algorithms on hybrid classical-quantum machines to solve certain classes of optimization problems. Algorithms proposed include the quantum approximate optimization algorithm (QAOA) [11], the quantum variational eigensolver (QVE) [25, 32] and variations and generalizations thereof, e.g., [27, 37]. Experimental demonstration of QVE for calculating the ground-state energy of small molecules has been reported in [17], while the application of QAOA for unsupervised learning of a clustering problem can be found in [29].

An alternative paradigm to the quantum gate-based approaches above is to harness the information processing capability of complex real-time quantum dynamics by introducing the so-called quantum reservoir computers (QRCs) [12, 28]. This approach is essentially a quantum implementation of classical *reservoir computing* schemes, in which a dynamical system processes an input sequence and produces an output sequence that approximates a target sequence, see, e.g., [16, 22, 24]. The main philosophy in reservoir computing is that the dynamics in arbitrary naturally occurring or engineered dynamical systems could potentially be exploited for computational purposes. In particular, a dynamical system could be used for computation without precise tuning or optimization of its parameters. To possess computational capability, the systems are required to satisfy three properties [24]: the *convergence property* [30], the *fading memory property* [6] and form a family of systems with the *separation property*. The convergence property ensures that computations performed by a dynamical system are independent of its initial condition, and the fading memory property implies that outputs of a dynamical system stay close if the corresponding inputs are close in recent times. The separation property states that there should be a member in the family of systems with dynamics sufficiently rich to distinguish any two different input sequences. Classical reservoir computing has been realized as simple nonlinear photonic circuits with a delay line [2] and in neuromorphic computing based on nanoscale oscillators [35], and it has been demonstrated to achieve state-of-the-art performance on applications such as spoken digit recognition [35].

Nonlinear input-output (I/O) maps with fading memory can be approximated by a series expansion such as the well-known Volterra series [6]. They can also be approximated by a family of classical nonlinear dynamical systems that have the three properties introduced in the previous paragraph. Such a family of dynamical systems is said to be *universal* (or possesses the universality property) for nonlinear I/O maps with fading memory. They include various classical reservoir computing schemes such as liquid state machines [24],

echo-state networks (ESNs) [13], and non-homogeneous state-affine systems [14]. However, a theoretical framework for the learning of nonlinear fading memory I/O maps by quantum systems is so far lacking. Moreover, an extended investigation into the potential advantage quantum systems offer over classical reservoir computing schemes has not been conducted. The provision of such a learning theory, the demonstration of a class of quantum model that is provably universal, and a study of this model via numerical experiments are the main contributions of this paper.

The paper is organized as follows. In Sec. II, we formally define fading memory maps. In Sec. III, we formulate the theory of learning nonlinear fading memory maps with dissipative quantum systems. Sec. IV introduces a concrete universal class of dissipative quantum systems. Sec. V numerically demonstrates the emulation performance of the proposed universal class in the absence and presence of decoherence. The effect of different input encodings on the learning capability of this class is investigated. An in-depth comparison between this universal class and ESNs is also conducted. We conclude this section by discussing the potential of this universal class to surpass classical schemes when implemented on a NISQ machine. Detailed results and numerical settings are collected in and can be found in the Appendix.

## II. FADING MEMORY MAPS

Let  $\mathbb{Z}$  denote the set of all integers and  $\mathbb{Z}^- = \{\dots, -1, 0\}$ . Let  $u = \{\dots, u_{-1}, u_0, u_1, \dots\}$  be a real bounded input sequence with  $\sup_{k \in \mathbb{Z}} |u_k| < \infty$ . We say that a real output sequence  $y = \{\dots, y_{-1}, y_0, y_1, \dots\}$  is related to  $u$  by a time-invariant causal map  $M$  if  $y_k = M(u|_k)$  for all  $k \in \mathbb{Z}$ . Here  $u|_k = \{\dots, u_{k-2}, u_{k-1}, u_k\}$  is the input sequence  $u$  truncated after time  $k$ .

For a fixed real positive constant  $L$  and a compact subset  $D \subseteq \mathbb{R}$ , we are interested in the set  $K_L(D)$  consisting of input sequences such that for all  $k \in \mathbb{Z}$ ,  $u_k \in D \cap [-L, L]$ . We say a time-invariant causal map  $M$  defined on  $K_L(D)$  has the fading memory property with respect to a decreasing sequence  $w = \{w_k\}$ ,  $\lim_{k \rightarrow \infty} w_k = 0$  if, for any two input sequences  $u$  and  $v$ ,  $|M(u|_0) - M(v|_0)| \rightarrow 0$  whenever  $\sup_{k \in \mathbb{Z}^-} |w_{-k}(u_k - v_k)| \rightarrow 0$ . In other words, if the elements of two sequences agree closely up to some recent past before  $k = 0$ , then their output sequences will also be close at  $k = 0$ .

## III. LEARNING NONLINEAR FADING MEMORY MAPS WITH DISSIPATIVE QUANTUM SYSTEMS

Since fading memory maps are time-invariant, any dynamical system that is used to approximate them must forget its initial condition. Classical dynamical systems with this property are referred to as *convergent systems* in control theory [30], and the property is known as the *echo state property* in the context of ESNs [8, 16]. For dissipative quantum systems, this means that for the same input sequence, density operators asymptotically converge to the same sequence of density operators, independently of their initial values. We emphasize that the dissipative nature of the quantum system is *essential* for the learning task. Without it the system clearly cannot be convergent.

Consider a quantum system consisting of  $n$  qubits with a Hilbert space of dimension  $2^n$

undergoing the following discrete-time dissipative evolution:

$$\rho_k = T(u_k)\rho_{k-1}, \quad (1)$$

for  $k = 1, 2, \dots$ , with initial condition  $\rho(0) = \rho_0$ . Here,  $\rho_k = \rho(k\tau)$  is the system density operator at time  $t = k\tau$  and  $\tau$  is a (fixed) sampling time, and  $T(u_k)$  is a completely positive trace preserving (CPTP) map for each  $u_k$ . In this setting, the real input sequence  $\{u_0, u_1, \dots\}$  determines the system's evolution. The overall input-output map in the long time limit is in general non-linear. Let  $\mathcal{D}(\mathbb{C}^{2^n})$  denote the convex set of all density operators on  $\mathbb{C}^{2^n}$ . In Appendix [VII A, Theorem 4], we show that if the CPTP map  $T : D \cap [-L, L] \rightarrow \mathcal{D}(\mathbb{C}^{2^n})$  is mixing and the induced operator norm of  $T$  on the hyperplane  $H_0$  of traceless Hermitian operators satisfies  $\|T(u_k)|_{H_0}\| < 1 - \epsilon$  for some  $\epsilon > 0$ , then it will forget its initial condition and is therefore convergent. This means that for any two initial density operators  $\rho_{j,0}$  ( $j = 1, 2$ ) and the corresponding density operators  $\rho_{j,k}$  at time  $t = k\tau$ , we will have that

$$\lim_{k \rightarrow \infty} \|\rho_{1,k} - \rho_{2,k}\| = \lim_{k \rightarrow \infty} \left\| \overleftarrow{\prod}_{j=0}^k T(u_j)(\rho_{1,0} - \rho_{2,0}) \right\| = 0,$$

where  $\overleftarrow{\prod}_{j=0}^k$  is a time-ordered composition of maps  $T(u_j)$  from right to left and  $\|\cdot\|$  is the Hilbert-Schmidt norm.

We introduce an output sequence  $\bar{y}$  in the form

$$\bar{y}_k = h(\rho_k), \quad (2)$$

where  $h : \mathcal{D}(\mathbb{C}^{2^n}) \rightarrow \mathbb{R}$  is a real functional of  $\rho_k$ . Eqs. (1) and (2) define a quantum dynamical system with input  $u$  and output  $\bar{y}$ . We now require the separation property. Consider a family  $\mathcal{F}$  of distinct quantum systems described by Eqs. (1) and (2), but possibly having differing number of qubits  $n$ . Let  $u$  and  $u'$  be two input sequences in  $K_L(D)$  that are not identical,  $u_k \neq u'_k$  for at least one  $k$ , and let  $\bar{y}$  and  $\bar{y}'$  be the respective outputs of the quantum system for these inputs. We say that the family  $\mathcal{F}$  is *separating* if for any non-identical inputs  $u$  and  $u'$  in  $K_L(D)$ , there exists a member in this family with non-identical outputs  $\bar{y}$  and  $\bar{y}'$ . As stated in Appendix [VII B, Theorem 9], any family of convergent dissipative quantum systems that implement fading memory maps with the separation property, and which forms an algebra of maps, is universal and can approximate any I/O map with fading memory arbitrarily closely.

#### IV. A UNIVERSAL CLASS OF DISSIPATIVE QUANTUM SYSTEMS

We now specify a class of dissipative quantum systems that is provably universal in approximating fading memory maps defined on  $K_1([0, 1])$ . The class consists of systems that are made up of  $N$  *non-interacting* sub-systems, with subsystem  $K$  consisting of  $n_K + 1$  qubits,  $n_K$  “system” qubits and a single “ancilla” qubit. We label the qubits of subsystem  $K$  by an index  $i_j^K$  that runs from  $j = 0$  to  $j = n_K$ , with  $i_0^K$  labeling the ancilla qubit. The  $n_K + 1$  qubits interact via the Hamiltonian

$$H_K = \sum_{j_1=0}^{n_K} \sum_{j_2=j_1+1}^{n_K} J_K^{j_1, j_2} (X^{(i_{j_1}^K)} X^{(i_{j_2}^K)} + Y^{(i_{j_1}^K)} Y^{(i_{j_2}^K)}) + \sum_{j=0}^{n_K} \alpha Z^{(i_j^K)},$$

where  $J_K^{j_1, j_2}$  and  $\alpha$  are real-valued constants, while  $X^{(i_j^K)}$ ,  $Y^{(i_j^K)}$  and  $Z^{(i_j^K)}$  are Pauli  $X$ ,  $Y$  and  $Z$  operators of qubit  $i_j^K$ . The ancilla qubits for all subsystems are periodically reset at time  $t = k\tau$  and prepared in the input-dependent mixed state  $\rho_{i_{0,k}}^K = u_k|0\rangle\langle 0| + (1-u_k)|1\rangle\langle 1|$  (with  $0 \leq u_k \leq 1$ ). The system qubits are initialized at time  $t = 0$  to some density operator. The density operator  $\rho_k^K$  of the  $K^{\text{th}}$  subsystem qubits evolves during time  $(k-1)\tau < t < k\tau$  according to  $\rho_k^K = T_K(u_k)\rho_{k-1}^K$ , where  $T_K(u_k)$  is the CPTP map defined by  $T_K(u_k)\rho_{k-1}^K = \text{Tr}_{i_0^K} \left( e^{iH_K\tau} \rho_{k-1}^K \otimes \rho_{i_{0,k}}^K e^{-iH_K\tau} \right)$  and  $\text{Tr}_{i_0^K}$  denotes the partial trace over the ancilla qubit of subsystem  $K$ . We now specify an output function  $h$  associated with this system. We will use a single index to label the system qubits from the  $N$  subsystems, the ancilla qubits are not used in the output. Consider an individual system qubit with index  $j$ , with  $j$  running from 1 until  $n = \sum_{j=1}^N n_j$ . The output functional  $h$  is defined to be of the general form,

$$\bar{y}_k = h(\rho_k) = C + \sum_{d=1}^R \sum_{i_1=1}^n \sum_{i_2=i_1+1}^n \cdots \sum_{i_n=i_{n-1}+1}^n \sum_{r_{i_1}+\cdots+r_{i_n}=d} w_{i_1, \dots, i_n}^{r_{i_1}, \dots, r_{i_n}} \langle Z^{(i_1)} \rangle_k^{r_{i_1}} \cdots \langle Z^{(i_n)} \rangle_k^{r_{i_n}} \quad (3)$$

where  $C$  is a constant,  $R$  is an integer and  $\langle Z^{(i)} \rangle_k = \text{Tr}(\rho_k Z^{(i)})$  is the expectation of the operator  $Z^{(i)}$ . We note that the functional  $h$  (the right hand side of the above) is a multivariate polynomial in the variables  $\langle Z^{(i)} \rangle_k$  ( $i = 1, \dots, n$ ) and these expectation values depend on input sequence  $\{u_k\}$ . Thus computing  $\bar{y}_k$  only involves estimating the expectations  $\langle Z^{(i)} \rangle_k$  and the degree of the polynomial  $R$  can be chosen as desired. If  $R = 1$  then  $\bar{y}_k$  is a simple linear function of the expectations.

This family of dissipative quantum systems exhibits two important properties, see Appendix VII C and VII D for the proofs. Firstly, if for each subsystem,  $T_K$  is mixing and  $T_K$  restricted to traceless Hermitian operators satisfies  $\|T_K(u_k)|_{H_0}\| < 1 - \epsilon$  for all  $u_k \in [0, 1]$  and some  $\epsilon > 0$ , then this family forms a polynomial algebra consisting of systems that implement fading memory maps. Secondly, a convergent single-qubit system with a linear output combination of expectation values (ie.  $N = 1$  and  $R = 1$ ), separates points of  $K_1([0, 1])$ . These two properties and an application of the Stone-Weierstrass Theorem [10, Theorem 7.3.1] guarantee the universality property.

The class specified above is a variant of the QRC model in [28] but is provably universal by the theory of the previous section. The differences are in the general form of the output and, in our model, the ancilla qubit is not used in computing the output. Also, we do not consider time-multiplexing. We remark that time-multiplexing can be in principle incorporated in the model using the same theory. However, this extension is more technical and will be pursued elsewhere.

## V. NUMERICAL EXPERIMENTS

We demonstrate the emulation performance of the universal class introduced above in learning nonlinear autoregressive moving average (NARMA) models, a class of models [3] that is often used to benchmark algorithms for learning time-series. NARMA is popular due to its dependency on time-lagged outputs and inputs, specified by the delay  $\tau_{\text{NARMA}}$ . Given  $\tau_{\text{NARMA}} = m$ , the corresponding task is denoted as NARMA $m$ . A randomly generated input sequence in the range  $[0, 0.2]$  is applied to all NARMA tasks. For each task, the experiment

firstly washes out the contribution of the initial condition, and is followed by a training and an evaluation phase, each consisting of 1000 timesteps.

We focus on quantum systems consisting of only a single subsystem ( $N = 1$ ) and the number of system qubits is small,  $n = \{2, 3, 4, 5, 6\}$ . We denote this class as SA. For all numerical experiments, the parameters of SA are chosen as follows. We introduce a scale  $S > 0$  such that the Hamiltonian parameters  $J^{j_1, j_2}/S$ ,  $h/S = 0.5$  and  $\tau S = 1$  are dimensionless. As for the QRCs in [12], we randomly generate  $J^{j_1, j_2}/S$  from  $[-1, 1]$  and, to ensure convergence, select the resulting Hamiltonians for experiments if the associated CPTP map is convergent. We analyze the performance during the evaluation phase using the normalized mean-squared error  $\text{NMSE} = \sum_{k=1}^{1000} (\bar{y}_k - y_k)^2 / \sum_{k=1}^{1000} y_k^2$ . For each task and each  $n$ , NMSEs of 100 convergent SAs are averaged for analysis.

In practical implementation, computation of the expectations  $\langle Z^{(j)} \rangle_k$  is offloaded to the quantum subsystem, and classical processing is needed only to optimize the output weights. For this reason, we associate the output weights  $w_i^{r_i}$  in Eq. (3) with *(classical) computational nodes*, with the number of such nodes being equal to the number of output weights. To avoid confusion, the constant  $C$  is not counted as a computational node, although in practice it can be viewed as one. The weight optimization is performed by standard least squares to minimize the mean-squared error  $\sum_k |y_k - \bar{y}_k|^2$ , where  $y$  is the target output sequence. The number of computational nodes for SA can be chosen arbitrarily by varying the degree  $R$  in the output, while the actual “dimension” of the state-space is  $2^n(2^{n+1} + 1) - 2^{n+1} = 2^n(2^{n+1} - 1)$ . This dimension corresponds to the number of real variables needed to describe the system density operator. On the other hand, for ESNs [16] and the Volterra series [6], the number of computational nodes and the dimension of the state-space are the same. For an ESN with  $m$  reservoir nodes ( $Em$ ), the number of computational nodes and the dimension of the state-space are  $m$ , while for the Volterra series with kernel order  $k$  and memory  $p$  ( $Vk, p$ ), they are defined as  $\frac{p^{k+1} - p}{p - 1}$ . We select  $m$  and  $(k, p)$  such that the number of computational nodes are less than 800. This reduces the chance of overfitting for learning a sequence of length 1000 [21]. For detailed experimental settings for the ESNs and Volterra series, see Appendix VII E.

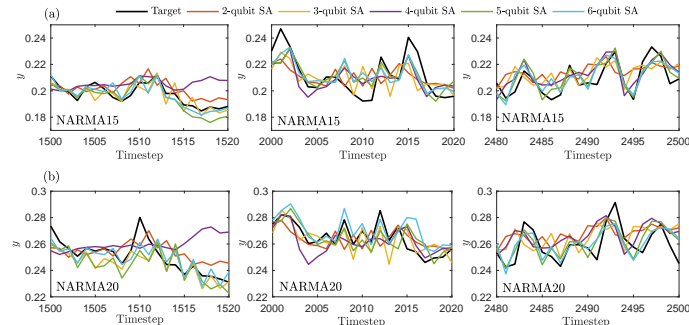


FIG. 1. Typical SA outputs during the evaluation phase, (a) the outputs for NARMA15 and (b) the outputs for NARMA20. The leftmost, middle and rightmost panels show the outputs for timesteps 1500-1520, 2000-2020 and 2490-2500 respectively

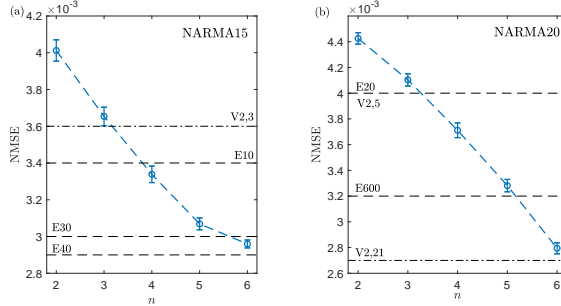


FIG. 2. Average SA NMSE for (a) NARMA15 and (b) NARMA20, the error bars represent the standard error. For comparison, horizontal dashed lines labeled with “Em” indicate the average performance of ESNs with  $m$  computational nodes, and horizontal dot-dashed lines labeled with “V $k, p$ ” indicates the performance of Volterra series with kernel order  $k$  and memory  $p$ . Overlapping dashed and dot-dashed lines are represented as dashed lines

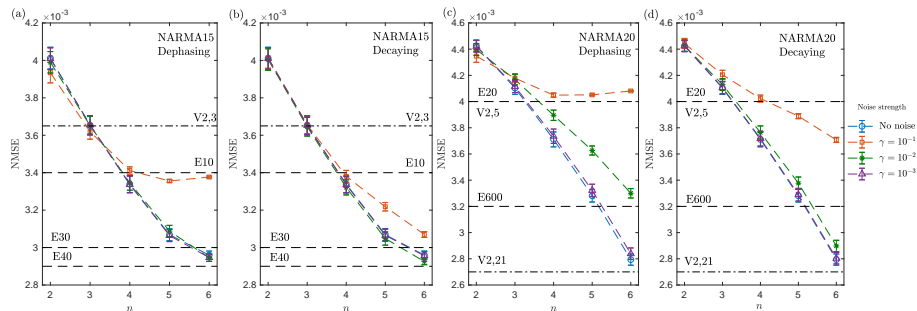


FIG. 3. Average SA NMSE for the NARMA tasks under decoherence. (a) and (b) are the average NMSE for NARMA15 in the presence of dephasing and decaying noise, respectively. (c) and (d) are the respective average NMSE for NARMA20 under dephasing and decaying noise. For comparison, the average SA NMSE without the effect of noise is also plotted. In all plots, the error bars represent the standard error

### A. Overview of SA learning performance

We present an overview of SA performance in learning NARMA15 and NARMA20, and compare its performance with ESNs and the Volterra series according to the number of computational nodes. We set  $R = 1$  in Eq. (3) such that the number of computational nodes coincides with the number of system qubits.

Fig. 1 shows the typical SA outputs for NARMA15 and NARMA20 during the evaluation phase and Fig. 2 plots the average SA NMSE as  $n$  increases. It is observed from Fig. 2 that the SA model with a small number of computational nodes performs comparably as ESNs and the Volterra series with a large number of computational nodes. For NARMA15, 3-qubit SA achieves a comparable performance as V2,3 with 12 computational nodes, and 6-qubit SA performs better than E30. For NARMA20, 6-qubit SA performs comparably as V2,21 with 462 computational nodes, and it outperforms E600. Our results are similar to the performance of the QRCs with time multiplexing reported in [12], where the QRCs are demonstrated to perform comparably as ESNs with a larger number of trainable

computational nodes.

It is also observed from Fig. 1 that as the number of system qubit increases, the SA output better approximates the target output. This is quantitatively confirmed in Fig. 2, which shows the average SA NMSE decreases as  $n$  increases. However, for the small number of qubits investigated, this rate of decrease is approximately linear despite the dimension of the Hilbert space increasing exponentially. For both the NARMA tasks, the average NMSEs for 2-qubit and 6-qubit SA are of the same order ( $10^{-3}$ ). A larger number of additional system qubits is required to substantially reduce the SA task error.

## B. SA performance under decoherence

We further validate the feasibility of the SA model in the presence of dephasing and decaying noise. Under dephasing noise, the density operator evolves according to  $\rho \rightarrow \frac{1+e^{-2\gamma\tau S}}{2}\rho + \frac{1-e^{-2\gamma\tau S}}{2}Z^{(j)}\rho Z^{(j)}$ . The decaying noise gives rise to the evolution  $\rho \rightarrow M_0^{(j)}\rho(M_0^{(j)})^\dagger + M_1^{(j)}\rho(M_1^{(j)})^\dagger$ , where  $M_l^{(j)}$  ( $l = 0, 1$ ) are the Kraus operators of the amplitude damping channel for qubit  $j$  and  $\dagger$  denotes the adjoint. We apply noise strengths  $\gamma/S = \{10^{-3}, 10^{-2}, 10^{-1}\}$ , which are within the experimentally feasible range for systems like NMR ensembles [36]. Fig. 3 indicates that for noise strengths  $\gamma/S = \{10^{-3}, 10^{-2}\}$ , both noise types do not significantly degrade SA task performance for the NARMA tasks. However, the impact of the noise strength  $\gamma/S = 10^{-1}$  is more pronounced, particularly for a larger number of system qubits. Dephasing noise is shown to degrade the SA learning performance more significantly than decaying noise with the same noise strength.

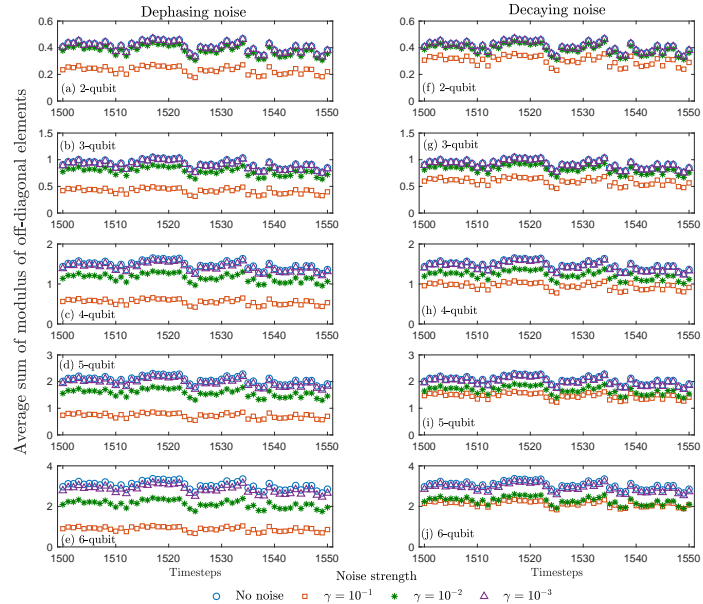


FIG. 4. Average sum of complex modulus of off-diagonal elements in the density operator under the dephasing noise (left) and the decaying noise (right)

A possible explanation for the behaviour of the SA model under the effect of decoherence is a loss of degrees of freedom, in the sense that off-diagonal elements of the density operator

become smaller and the density operator looks more like a classical probability distribution. Alternatively, this could be viewed as the off-diagonal elements contributing less to the overall computation in the dissipative quantum system. To support this explanation, for each  $n$ , we sum the modulus of off-diagonal elements in the density operator for the 100  $n$ -qubit SA samples simulated above, in the NARMA20 learning task. The average of these 100 sums is plotted for the first 50 timesteps in the evaluation phase in Fig. 4. That is, Fig. 4 plots  $\frac{2}{n_s} \sum_{l=1}^{n_s} \sum_{r=1}^{2^n} \sum_{s=r+1}^{2^n} |\rho_{k,rs}^{(l)}|$ , where  $n_s = 100$  is the number of different random SA models sampled and  $\rho_{k,rs}^{(l)}$  denotes the element of  $\rho_k^{(l)}$  in row  $r$  and column  $s$  (the superscript  $(l)$  indexing the SA sample).

Fig. 4 shows that as the dephasing noise strength increases, the sum decreases significantly, particularly with the noise strength  $\gamma/S = 10^{-1}$ . However, in the presence of the decaying noise, the sum does not vary noticeably as the noise strength changes, confirming that decaying noise has less impact on the learning performance of SA. The observed trend for the average sum persists as the timestep increases to 2500 (see Appendix VII E 2). The results presented in Fig. 4 further indicate that though the output of SA depends solely on the diagonal elements of the density operator (this follows from (3)), nonzero off-diagonal elements are crucial for improving the SA emulation performance. This provides a plausible explanation for the improved performance achieved by increasing the number of qubits, thereby increasing Hilbert space size and the number of non-zero off-diagonal elements. Further investigation into this topic is presented in Sec. V D.

### C. Effect of different input encodings

Our proposed universal class encodes the input  $u_k \in [0, 1]$  into the mixed state  $\rho_{i_0,k} = u_k|0\rangle\langle 0| + (1 - u_k)|1\rangle\langle 1|$ . Other input encoding possibilities include the pure state  $\rho_{i_0,k} = (\sqrt{u_k}|0\rangle + \sqrt{1 - u_k}|1\rangle)(\sqrt{u_k}\langle 0| + \sqrt{1 - u_k}\langle 1|)$  used in the QRC model [12], encoding the input into the phase  $\rho_{i_0,k} = \frac{1}{2}(|0\rangle + e^{-iu_k}|1\rangle)(\langle 0| + e^{iu_k}\langle 1|)$ , and encoding the input into non-orthogonal basis  $\rho_{i_0,k} = u_k|0\rangle\langle 0| + \frac{1-u_k}{2}(|0\rangle + |1\rangle)(\langle 0| + \langle 1|)$ . We denote these different input encodings as mixed, pure, phase and non-orthogonal. However, we emphasize that for the last three encodings the universality of the associated dissipative quantum system using these encodings has not been proven.

To investigate the impact of input encodings on the computational capability of quantum systems, the Hamiltonian parameters are sampled from the same uniform distribution, and the resulting Hamiltonians are chosen if the associated CPTP map that implements the specified input-dependent density operator  $\rho_{i_0,k}$  is convergent. For each input encoding, NMSEs of 100 convergent systems are averaged for analysis. Fig. 5 shows that the average NMSEs for different input encodings for both the NARMA tasks are of the same order ( $10^{-3}$ ). Moreover, as the number of system qubits increases, the errors of different input encodings decrease at roughly the same rate. This comparison indicates that the effect of different input encodings on the learning performance does not appear significant.

### D. Further comparison with ESNs

Our numerical results so far and the results shown in [12] both suggest that dissipative quantum systems with a small number of qubits achieve comparable performance to classical learning schemes with a large number of computational nodes. However, these comparisons

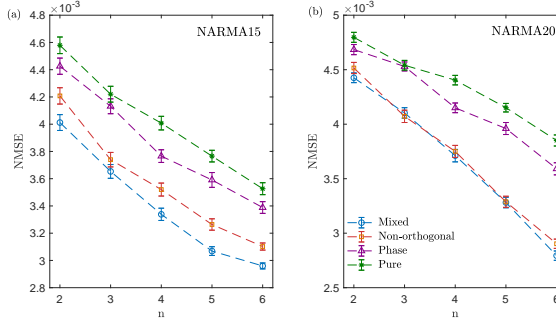


FIG. 5. Average NMSEs for different input encodings, (a) average NMSEs for NARMA15 and (b) average NMSEs for NARMA20. Error bars represent the standard error

TABLE 1. Average SA and E496 NMSE for the NARMA tasks. Results are rounded to two significant figures. The notation ( $\pm$  se) denotes the standard error

$\tau_{\text{NARMA}}$	SA NMSE ( $\pm$ se)	E496 NMSE ( $\pm$ se)
15	$3.3 \times 10^{-3} \pm 4.4 \times 10^{-5}$	$2.2 \times 10^{-3} \pm 4.1 \times 10^{-7}$
20	$3.7 \times 10^{-3} \pm 5.6 \times 10^{-5}$	$3.3 \times 10^{-3} \pm 9.7 \times 10^{-7}$
30	$9.9 \times 10^{-3} \pm 1.1 \times 10^{-4}$	$9.1 \times 10^{-3} \pm 9.2 \times 10^{-7}$
40	$12 \times 10^{-3} \pm 1.4 \times 10^{-4}$	$11 \times 10^{-3} \pm 4.3 \times 10^{-6}$

may appear to be skewed favorably towards quantum dynamical systems, since it does not address their exponential state-space size. One can, for example, also increase the state-space size of ESNs and the number of computational nodes of SA, such that the state-space size and the number of computational nodes are the same for both models. Here we present a further comparison between the SA model and ESNs, and provide insights on the possible advantage SA might offer over its classical counterpart.

We focus on 4-qubit SA with a state-space size of 496. Setting  $R = 8$  in Eq. (3), the number of computational nodes for SA is 494, approximately the same as its state-space size. We compare this 4-qubit SA average task performance for NARMA15, NARMA20, NARMA30 and NARMA40 with the average E496 task performance. As shown in Table 1, the task error for both models are of the same order ( $10^{-3}$ ). However, E496 has a smaller error in each task. This comparison suggests that when the state-space size and the number of computational nodes for both models are similar, ESNs can outperform SA.

We further investigate under what conditions SA might offer a computational advantage. We observe that while the number of computational nodes is kept constant, increasing the state-space size of SA induces a considerable computational improvement. To demonstrate this, 4-, 5- and 6-qubit SA are simulated to approximate NARMA15, NARMA20, NARMA30 and NARMA40. For each  $n$ -qubit SA, we vary its output degree  $R$  such that its number of computational nodes ranges from 4 to 494. The chosen degrees for 4-qubit SA are  $R_4 = \{1, \dots, 8\}$ , for 5-qubit are  $R_5 = \{1, \dots, 6\}$ , and for 6-qubit SA are  $R_6 = \{1, \dots, 5\}$ . For each  $n$ -qubit SA, the Hamiltonians are the same for all its chosen output degrees, and the task errors of 100 convergent SA models are averaged for analysis.

For comparison, we simulate 100 convergent ESNs with reservoir size 496 to learn the NARMA tasks. For  $n$ -qubit SA, let  $C_n$  ( $n = 4, 5, 6$ ) denotes the numbers of computational

nodes corresponding to its output degrees  $R_n$ . The number of computational nodes for E496 is set to  $C_4 \cup C_5 \cup C_6$ . When the number of computational nodes is smaller than the space-state size of E496, we select the computational nodes corresponding to the most representative state elements. For instance, suppose that we set the number of computational nodes for E496 to be 4. During the training phase, 496 output weights are obtained via standard least squares. Then 4 weights with the largest absolute values and their corresponding elements from the state-space are selected. These 4 state elements are used to re-optimize 4 output weights. During the evaluation phase, 496 state elements evolve, but only the 4 most representative state elements and the 4 output weights are used for computing the E496 output.

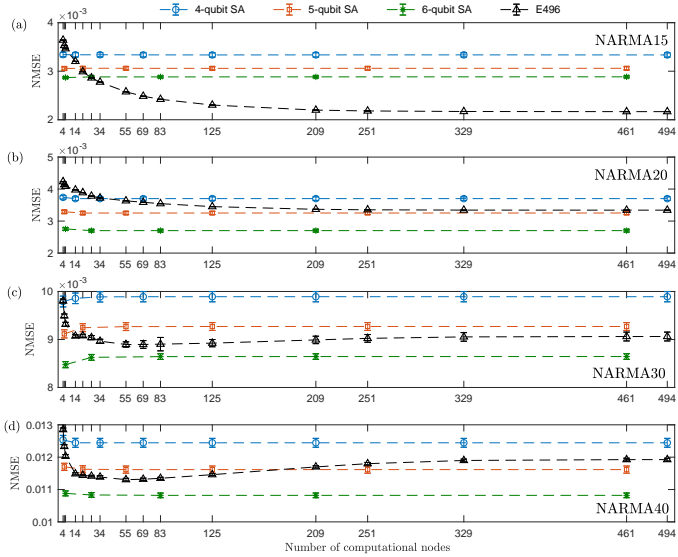


FIG. 6. Average SA NMSE as the state-space size and the number of computational nodes vary for the NARMA tasks. The average NMSE for E496 with the corresponding number of computational nodes is plotted for comparison

Fig. 6 plots the 4-, 5-, and 6-qubit SA average NMSEs as the number of computational nodes increases for the NARMA tasks. For comparison, the average E496 NMSE is also plotted. Two important observations are that increasing the number of computational nodes does not improve SA task performance, while increasing the state-space size induces a noticeable improvement in the NMSE. For NARMA20 and 461 computational nodes, the average NMSE for 5-qubit SA is  $3.4 \times 10^{-3}$  whereas the average NMSE for 6-qubit SA is  $2.8 \times 10^{-3}$ . This improvement due to the increasing state-space size is more significant as the delay for the NARMA task increases. When comparing to E496, we observe that despite 4-qubit SA performing worse than E496, subsequent increases in the state-space size allows the SA model to outperform E496, without extensively increasing its number of computational nodes.

Contrary to the above observations for the SA model, increasing the reservoir size of ESNs while keeping the number of output weights fixed does not induce a significant computational improvement. To numerically demonstrate this, the reservoir size of ESNs is further

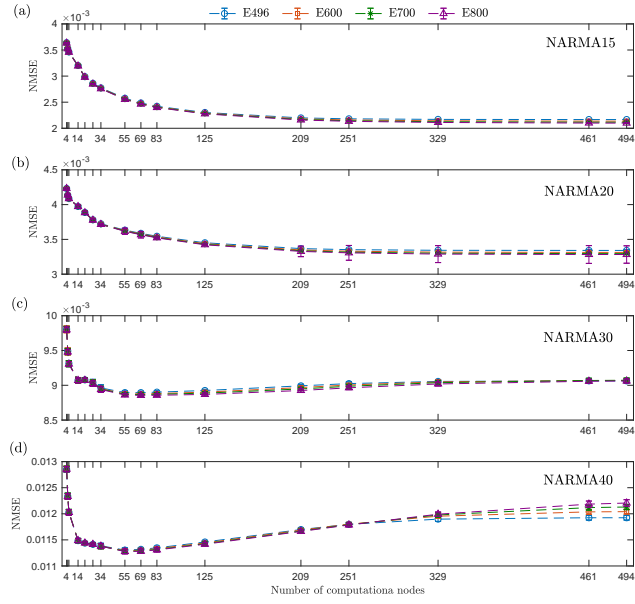


FIG. 7. Average ESNs NMSE as the state-space size and the number of computational nodes vary for the NARMA tasks

increased to  $\{600, 700, 800\}$ . For each reservoir size, the number of computational nodes is set to be the same as that of E496. These computational nodes are chosen and optimized by the method described above for the E496. We average the task errors of 100 convergent ESNs for each reservoir size. As shown in Fig. 7, noticeable performance improvements for ESNs are only observed as the number of computational nodes increases, but not as the reservoir size varies.

The above observations have several implications. To improve the computational capability of the SA model, one can take advantage of the exponentially increasing state-space size while only optimizing a polynomial number of computational nodes. In contrary, to improve the computational capability of ESNs, one needs to increase the number of computational nodes, which is upper bounded by the reservoir size. Therefore, enhancing emulation performance of ESNs inevitably requires the state-space size to be increased. In the situation when the state-space size increases beyond what classical computers can simulate in a reasonable amount of time and with reasonable resources (such as memory), the computational capability of ESNs saturates, whereas the computational capability of the SA model could be further improved by increasing the number of qubits in a linear fashion. In this regime, the SA model could provide a potential computational advantage over its classical counterpart. To further verify the feasibility of this hypothesis, the learning capability of the SA model would need to be evaluated for a larger number of qubits on a physical quantum system. A possible implementation of this experiment is on NMR ensembles, as suggested in [12]. However, motivated by the availability of NISQ machines, a quantum circuit implementation of the SA model, using the schemes proposed in [5, 15], would be more attractive. This is another topic of further research continuing from this work.

## VI. CONCLUSION AND OUTLOOK

We have developed a general theory for learning arbitrary I/O maps with fading memory using dissipative quantum systems. The attractiveness of the theory studied here is that it allows a dissipative quantum system (that meet certain requirements but is otherwise arbitrary) to be combined with a classical processor to learn I/O maps from sample I/O sequences. We apply the theory to demonstrate a universal class of dissipative quantum systems that can approximate arbitrary I/O maps with fading memory.

Numerical experiments on the NARMA tasks indicate that even with only a small number of qubits and a simple linear output, this class can achieve comparable performance, in terms of the average mean squared error, to classical learning schemes such as ESNs and the Volterra series with a large number of tunable parameters. However, when the state-space sizes of the quantum subsystem and classical learning schemes are the same, and the same number of computational nodes are used, the quantum system does not demonstrate any computational advantage. Moreover, the numerical results for a small number of qubits indicate that increasing the dimension of the Hilbert space of the quantum system while fixing the number of computational nodes can still result in improved prediction performance on the NARMA benchmarking tasks, whereas increasing the state space of ESNs while fixing the computational nodes does not lead to any noticeable improvement. This strongly suggests that the possibly very large Hilbert space of the quantum subsystem presents a potential resource that can be exploited in this approach. That is, for state-space dimensions beyond what can be simulated on a conventional digital computer. It remains to be investigated if this resource can indeed lead to a provable performance advantage over conventional classical learning approaches, and the circumstances where this will be the case.

## VII. APPENDIX

### A. The convergence property

Recall from the main text that for a compact set  $D \subset \mathbb{R}$  and positive integer  $L$ ,  $K_L(D)$  denotes the set of all real sequences  $\{u_k\}_{k \in \mathbb{Z}}$  taking values in  $D \cap [-L, L]$ . We let  $K_L^-(D)$  and  $K_L^+(D)$  to be subsets of input sequences in  $K_L(D)$  whose indices are restricted to the sets  $\mathbb{Z}^- = \{\dots, -2, -1, 0\}$  and  $\mathbb{Z}^+ = \{0, 1, 2, \dots\}$ , respectively. In the following, we write  $T$  for both input-independent and input-dependent CPTP maps. If the input  $u_k$  is specified for an input-dependent CPTP map, we denote it as  $T(u_k)$ . We now state the definition of a convergent CPTP map with respect to  $K_L(D)$ .

**Definition 1** (Convergence). *An input-dependent CPTP map  $T$  is convergent with respect to  $K_L(D)$  if for all  $u \in K_L^+(D)$ , there exists a sequence  $\delta = \{\delta_k\}$  with  $\lim_{k \rightarrow \infty} \delta_k = 0$  such that for any two density operators  $\rho_{j,k}$  ( $j = 1, 2$ ) satisfying  $\rho_{j,k} = T(u_k)\rho_{j,k-1}$ , it holds that  $\|\rho_{1,k} - \rho_{2,k}\| \leq \delta_k$ . We call a dissipative quantum system whose dynamics is governed by a convergent CPTP map a convergent system.*

A sufficient condition for a CPTP map to be convergent is mixing, a concept from statistical dynamics of noisy quantum channel [34].

**Definition 2** (Mixing). A CPTP map  $T$  is mixing if for all  $\rho_0 \in \mathcal{D}(\mathbb{C}^{2^n})$ , there exists a unique density operator  $\rho_*$  such that

$$\lim_{k \rightarrow \infty} \left\| \prod_{j=0}^k T(\rho_0) - \rho_* \right\| = 0.$$

One can characterize the mixing condition in terms of the spectral property of a CPTP map acting on  $\mathcal{L}(\mathbb{C}^{2^n})$ , the set of all linear operators on  $\mathbb{C}^{2^n}$ . In this light, a CPTP map is mixing if and only if eigenvalue  $\lambda = 1$  is simple and is the only eigenvalue satisfying  $|\lambda| = 1$  [9, Theorem 7]. We immediately have the following corollary.

**Corollary 3.** For a mixing CPTP map  $T$ , denote the set of fixed points of  $T$  to be  $\mathcal{P}_T = \{A \in \mathcal{L}(\mathbb{C}^{2^n}) \mid T(A) = A\}$ . Then  $\mathcal{P}_T = \text{span}\{\rho_*\}$ , where  $\rho_*$  is the unique density operator given in Definition 2.

For an input-independent CPTP map, mixing trivially implies convergence. For an input-dependent CPTP map, an additional condition on  $\|T\| = \sup_{\substack{A \in \mathcal{L}(\mathbb{C}^{2^n}) \\ \|A\|=1}} \|T(A)\|$ , the operator norm induced by the Hilbert-Schmidt norm, is required.

**Theorem 4** (Convergence property). Let  $u \in K_L^+(D)$ , suppose that for all  $k \in \mathbb{Z}^+$ ,  $T(u_k)$  is mixing and the restriction of  $T$  to the hyperplane  $H_0$  of traceless Hermitian operators  $T|_{H_0}$  satisfies  $\|T(u_k)|_{H_0}\| < 1 - \epsilon$  for some  $\epsilon > 0$ . Then  $T$  is convergent with respect to  $K_L(D)$  and any pair of initial density operators converge uniformly to one another under  $T$ .

*Proof.* Let  $\rho_{1,0}$  and  $\rho_{2,0}$  be two arbitrary initial density operators,  $\rho_{1,0} - \rho_{2,0}$  is a traceless Hermitian operator. Since  $T(u_j)$  is mixing for all  $j \in \mathbb{Z}^+$ , by Corollary 3,  $\rho_{1,0} - \rho_{2,0} \notin \mathcal{P}_{T(u_j)}$ . Therefore,

$$\begin{aligned} \|\rho_{1,k} - \rho_{2,k}\| &= \left\| \overleftarrow{\prod}_{j=0}^k T(u_j)(\rho_{1,0} - \rho_{2,0}) \right\| \\ &= \left\| \overleftarrow{\prod}_{j=0}^k T(u_j)|_{H_0}(\rho_{1,0} - \rho_{2,0}) \right\| \\ &\leq \overleftarrow{\prod}_{j=0}^k \|T(u_j)|_{H_0}\| \|\rho_{1,0} - \rho_{2,0}\| \\ &< \overleftarrow{\prod}_{j=0}^k (1 - \epsilon) \|\rho_{1,0} - \rho_{2,0}\| \\ &\leq (1 - \epsilon)^{k+1} (\|\rho_{1,0}\| + \|\rho_{2,0}\|) \\ &\leq 2(1 - \epsilon)^{k+1}, \end{aligned}$$

where the last inequality results from the fact that for all  $\rho \in \mathcal{D}(\mathbb{C}^{2^n})$ ,  $\|\rho\|^2 = \text{Tr}(\rho^2) \leq 1$ .  $\square$

## B. The universality property

We now show the universality property of convergent dissipative quantum systems. Let  $\mathbb{R}^{\mathbb{Z}}$  be the set of all real-valued sequences. For a convergent dissipative quantum system

described by Eqs. (1) and (3) in the main text, we define the induced filter as  $M_h^T : K_L(D) \rightarrow \mathbb{R}^{\mathbb{Z}}$  such that for any initial condition  $\rho_{-\infty} \in \mathcal{D}(\mathbb{C}^{2^n})$ , when evaluated at time  $t = k\tau$ ,

$$M_h^T(u)|_k = M_h^T(u|_k) = h(\overrightarrow{\prod}_{j=0}^{\infty} T(u_{k-j})\rho_{-\infty}),$$

where  $\overrightarrow{\prod}_{j=0}^{\infty} T(u_{k-j}) = \lim_{N \rightarrow \infty} \overleftarrow{\prod}_{j=0}^N T(u_{k+(j-N)}) = \lim_{N \rightarrow \infty} T(u_k)T(u_{k-1}) \cdots T(u_{k-N})$ , and the limit is a point-wise limit. This filter is causal since given  $u, v \in K_L(D)$  satisfying  $u_{\tau} = v_{\tau}$  for  $\tau \leq k$ ,  $M_h^T(u)|_k = M_h^T(v)|_k$ .

For any  $\tau \in \mathbb{Z}$ , let  $M_{\tau}$  be the shift operator defined by  $M_{\tau}(u)|_k = u_{k-\tau}$ . A filter is said to be time-invariant if it commutes with  $M_{\tau}$ . It is straightforward to show that  $M_h^T$  is time-invariant.

For a time-invariant and causal filter, there is a corresponding functional  $F_h^T : K_L^-(D) \rightarrow \mathbb{R}$  defined as  $F_h^T(u) = M_h^T(u)|_0$  (see [6]). The corresponding filter can be recovered via  $M_h^T(u)|_k = F_h^T(P \circ M_{-k}(u))$ , where  $P$  truncates  $u$  up to 0, that is  $P(u) = u|_0$ . We say a filter  $M_h^T$  has the fading memory property if and only if  $F_h^T$  is continuous with respect to a weighted norm defined as follows.

**Definition 5** (Weighted norm). *For a null sequence  $w$ , that is  $w : \mathbb{N} \rightarrow (0, 1]$  is decreasing and  $\lim_{k \rightarrow \infty} w_k = 0$ , define a weighted norm  $\|\cdot\|_w$  on  $K_L^-(D)$  as  $\|u\|_w = \sup_{k \in \mathbb{Z}^-} |u_k| w_{-k}$ .*

**Definition 6** (Fading memory). *A time-invariant causal filter  $M : K_L(D) \rightarrow \mathbb{R}^{\mathbb{Z}}$  has the fading memory property with respect to a null sequence  $w$  if and only if the corresponding functional  $F : K_L^-(D) \rightarrow \mathbb{R}$  is continuous with respect to the weighted norm  $\|\cdot\|_w$ .*

To emphasize that the fading memory is defined with respect to a null sequence  $w$ , we will say that  $M$  is a *w-fading memory filter* and the corresponding functional  $F$  is a *w-fading memory functional*. We state the following compactness result [14, Lemma 2.2] and the Stone-Weierstrass theorem [10, Theorem 7.3.1].

**Lemma 7** (Compactness). *For any null sequence  $w$ ,  $K_L^-(D)$  is compact with the weighted norm  $\|\cdot\|_w$ .*

**Theorem 8** (Stone-Weierstrass). *Let  $E$  be a compact metric space and  $C(E)$  be the set of real-valued continuous functions on  $E$ . If a subalgebra  $A$  of  $C(E)$  contains the constant functions and separates points of  $E$ , then  $A$  is dense in  $C(E)$ .*

Let  $C(K_L^-(D), \|\cdot\|_w)$  be the set of continuous functionals  $F : (K_L^-(D), \|\cdot\|_w) \rightarrow \mathbb{R}$ . We have the following theorem as a result of the compactness of  $(K_L^-(D), \|\cdot\|_w)$  (Lemma 7) and the Stone-Weierstrass Theorem (Theorem 8).

**Theorem 9.** *Let  $w$  be a null sequence. For a convergent  $T$ , let  $\mathcal{M}_w = \{M_h^T \mid h : \mathcal{D}(\mathbb{C}^{2^n}) \rightarrow \mathbb{R}\}$  be the set of *w-fading memory filters*. Let  $\mathcal{F}_w$  be the family of corresponding functionals defined on  $K_L^-(D)$ . If  $\mathcal{F}_w$  forms a polynomial algebra of  $C(K_L^-(D), \|\cdot\|_w)$ , contains constants and separates points of  $K_L^-(D)$ , then  $\mathcal{F}_w$  is dense in  $C(K_L^-(D), \|\cdot\|_w)$ . That is for any time-invariant causal filter  $M_*$  that has *w-fading memory*, there exists  $M_h^T \in \mathcal{M}_w$  such that for any  $\epsilon > 0$  and all  $u \in K_L(D)$ ,  $\|M_*(u) - M_h^T(u)\|_{\infty} = \sup_{u \in K_L(D)} |M_*(u) - M_h^T(u)| < \epsilon$ .*

*Proof.*  $\mathcal{F}_w$  is dense follows from Lemma 7 and Theorem 8. To prove the second part of the theorem, since  $\mathcal{F}_w$  is dense in  $C(K_L^-(D), \|\cdot\|_w)$ , for any  $\epsilon > 0$  and any *w-fading memory*

functional  $F_*$ , there exists  $F_h^T \in \mathcal{F}_w$  such that for all  $u_- \in K_L^-(D)$ ,  $|F_*(u_-) - F_h^T(u_-)| < \epsilon$ . For  $u \in K_L(D)$ , notice that  $P \circ M_{-k}(u) \in K_L^-(D)$  for all  $k \in \mathbb{Z}$ , hence

$$\sup_{k \in \mathbb{Z}} |F_*(P \circ M_{-k}(u)) - F_h^T(P \circ M_{-k}(u))| = \sup_{k \in \mathbb{Z}} |M_*(u)|_k - M_h^T(u)|_k| < \epsilon.$$

Since this is true for all  $k \in \mathbb{Z}$ , thus for all  $u \in K_L(D)$ ,  $\|M_*(u) - M_h^T(u)\|_\infty < \epsilon$ .  $\square$

### C. Fading memory property and polynomial algebra

Before we prove the universality of the family of dissipative quantum systems introduced in Sec. IV in the main text, we first show two important observations regarding to the multivariate polynomial output in Eq. (3).

We specify  $h$  to be the multivariate polynomial as in the right hand side of Eq. (3) in the main text. For the ease of notation, we drop the subscript  $h$  in  $F_h^T$  and  $M_h^T$ . Let  $\mathcal{F} = \{F^T\}$  be the set of functionals induced from dissipative quantum systems given by Eqs. (1) and (3) in the main text. We will show in Lemma 10 that the convergence and continuity of  $T$  are sufficient to guarantee the fading memory property of  $F^T$ , and in Lemma 12 that  $\mathcal{F}$  forms a polynomial algebra, made of fading memory functionals.

**Lemma 10** (Fading memory property). *Suppose  $T$  satisfies the conditions in Theorem 4 so that it is convergent, and  $T(x)$  is continuous in the operator norm with respect to  $x$  for all  $x \in [-L, L] \cap D$ . That is for any  $\epsilon > 0$  and  $x, y \in [-L, L] \cap D$ , if  $|x - y| < \delta_T(\epsilon)$ , then  $\|T(x) - T(y)\| < \epsilon$ . Then for any null sequence  $w$ , the filter  $M^T$  and the corresponding functional  $F^T$  induced by dissipative quantum systems given by Eqs. (1) and (3) in the main text are  $w$ -fading memory.*

*Proof.* We first state the boundedness of CPTP maps [31, Theorem II.1].

**Lemma 11.** *For a CPTP map  $T : \mathcal{D}(\mathbb{C}^{2^n}) \rightarrow \mathcal{D}(\mathbb{C}^{2^n})$ , we have  $\|T\| \leq \sqrt{2^n}$ .*

Moreover, recall that  $\text{Tr}(\cdot)$  is continuous, that is for any  $\epsilon > 0$ , given  $A, B \in \mathcal{L}(\mathbb{C}^{2^n})$  such that  $\|A - B\| < \delta_{\text{Tr}}(\epsilon)$ , then  $|\text{Tr}(A - B)| < \epsilon$ .

Let  $w$  be an arbitrary null sequence. We will show the linear terms  $L(u)$  in the functional  $F^T$  are continuous with respect to  $\|\cdot\|_w$ , and the continuity property of  $F^T$  follows from the fact that finite sums and products of continuous elements are also continuous.

For any  $u, v \in K_L^-(D)$ ,

$$|L(u) - L(v)| = \left| \text{Tr} \left( Z^{(i_1)} \left( \overrightarrow{\prod}_{k=0}^{\infty} T(u_{-k}) \rho_{-\infty} - \overrightarrow{\prod}_{k=0}^{\infty} T(v_{-k}) \rho_{-\infty} \right) \right) \right|.$$

Denote  $\rho_u = \overrightarrow{\prod}_{k=N}^{\infty} T(u_{-k}) \rho_{-\infty}$  and  $\rho_v = \overrightarrow{\prod}_{k=N}^{\infty} T(v_{-k}) \rho_{-\infty}$  for some  $N > 0$ ,

$$\begin{aligned} & \left\| Z^{(i_1)} \left( \overrightarrow{\prod}_{k=0}^{\infty} T(u_{-k}) \rho_{-\infty} - \overrightarrow{\prod}_{k=0}^{\infty} T(v_{-k}) \rho_{-\infty} \right) \right\| \\ & \leq \|Z^{(i_1)}\| \left( \left\| \overrightarrow{\prod}_{k=0}^{N-1} T(u_{-k}) - \overrightarrow{\prod}_{k=0}^{N-1} T(v_{-k}) \right\| \|\rho_u\| + \left\| \overrightarrow{\prod}_{k=0}^{N-1} T(v_{-k}) (\rho_u - \rho_v) \right\| \right). \end{aligned} \quad (4)$$

Since  $T$  satisfies conditions in Theorem 4, for any  $\epsilon > 0$ , there exists  $N(\epsilon) > 0$  such that for all  $N' > N(\epsilon)$ ,

$$\left\| \overrightarrow{\prod}_{k=0}^{N'} T(v_{-k})(\rho_u - \rho_v) \right\| < \frac{\delta_{\text{Tr}}(\epsilon)}{2 \|Z^{(i_1)}\|}. \quad (5)$$

Choose  $N' = N(\epsilon) + 1$ , bound the first term in the sum of Eq. (4) by rewriting it as a telescopic sum:

$$\begin{aligned} & \left\| \overrightarrow{\prod}_{k=0}^{N(\epsilon)} T(u_{-k}) - \overrightarrow{\prod}_{k=0}^{N(\epsilon)} T(v_{-k}) \right\| \\ &= \left\| \sum_{l=0}^{N(\epsilon)} (T(v_0) \cdots T(v_{-(l-1)}) T(u_{-l}) T(u_{-(l+1)}) \cdots T(u_{-N(\epsilon)})) \right. \\ &\quad \left. - T(v_0) \cdots T(v_{-(l-1)}) T(v_{-l}) T(u_{-(l+1)}) \cdots T(u_{-N(\epsilon)}) \right\| \\ &\leq \sum_{l=0}^{N(\epsilon)} \|T(v_0) \cdots T(v_{-(l-1)})\| \|T(u_{-l}) - T(v_{-l})\| \|T(u_{-(l+1)}) \cdots T(u_{-N(\epsilon)})\| \\ &\leq 2^n \sum_{l=0}^{N(\epsilon)} \|T(u_{-l}) - T(v_{-l})\|, \end{aligned} \quad (6)$$

where the last inequality follows from Lemma 11. We claim that for any  $\epsilon > 0$ , if

$$\|u - v\|_w = \sup_{k \in \mathbb{Z}^-} |u_k - v_k| w_{-k} < \delta_T \left( \frac{\delta_{\text{Tr}}(\epsilon)}{2^{n+1} \|Z^{(i_1)}\| (N(\epsilon) + 1)} \right) w_{N(\epsilon)}$$

then  $|L(u) - L(v)| < \epsilon$ . Indeed, since  $w$  is decreasing, the above condition implies that

$$\max_{0 \leq l \leq N(\epsilon)} |u_{-l} - v_{-l}| w_{N(\epsilon)} < \delta_T \left( \frac{\delta_{\text{Tr}}(\epsilon)}{2^{n+1} \|Z^{(i_1)}\| (N(\epsilon) + 1)} \right) w_{N(\epsilon)}.$$

Since  $w_{N(\epsilon)} > 0$ , for all  $0 \leq l \leq N(\epsilon)$ ,

$$|u_{-l} - v_{-l}| < \delta_T \left( \frac{\delta_{\text{Tr}}(\epsilon)}{2^{n+1} \|Z^{(i_1)}\| (N(\epsilon) + 1)} \right).$$

By continuity of  $T$ , we bound Eq. (6) by

$$2^n \sum_{l=0}^{N(\epsilon)} \|T(u_{-l}) - T(v_{-l})\| < 2^n \sum_{l=0}^{N(\epsilon)} \frac{\delta_{\text{Tr}}(\epsilon)}{2^{n+1} \|Z^{(i_1)}\| (N(\epsilon) + 1)} = \frac{\delta_{\text{Tr}}(\epsilon)}{2 \|Z^{(i_1)}\|}. \quad (7)$$

Since  $\|\rho_u\| \leq 1$ , Eqs. (4), (5) and (7) give

$$\|Z^{(i_1)}\| \left( \left\| \overrightarrow{\prod}_{k=0}^{N(\epsilon)} T(u_{-k}) - \overrightarrow{\prod}_{k=0}^{N(\epsilon)} T(v_{-k}) \right\| \|\rho_u\| + \left\| \overrightarrow{\prod}_{k=0}^{N(\epsilon)} T(v_{-k})(\rho_u - \rho_v) \right\| \right) < \delta_{\text{Tr}}(\epsilon).$$

The result now follows from the continuity of  $\text{Tr}(\cdot)$ .  $\square$

**Lemma 12** (Polynomial algebra). *For any null sequence  $w$ , the family of functionals  $\mathcal{F} = \{F^T\}$  induced by dissipative quantum systems defined by Eqs. (1) and (3) in the main text, where  $T$  satisfies conditions in Theorem 4 and  $T(x)$  is continuous in the operator norm with respect to  $x$  for all  $x \in [-L, L] \cap D$ , forms a polynomial algebra consisting of  $w$ -fading memory functionals.*

*Proof.* Consider two dissipative quantum systems described by Eqs. (1) and (3), with  $n_1$  and  $n_2$  system qubits respectively. Let  $\rho_k^{(m)} \in \mathcal{D}(\mathbb{C}^{2^{n_m}})$  be the state and  $T^{(m)}$  be the CPTP map of the  $m^{\text{th}}$  system. Let  $j_1 = 1, \dots, n_1$  and  $j_2 = 1, \dots, n_2$  be the respective qubit index for the two systems. For any observable  $Z^{(j_m)}$  of qubit  $j_m$ , notice that

$$\begin{aligned}\text{Tr}\left(Z^{(j_1)}\rho_k^{(1)}\right) &= \text{Tr}\left((Z^{(j_1)} \otimes I)(\rho_k^{(1)} \otimes \rho_k^{(2)})\right), \\ \text{Tr}\left(Z^{(j_2)}\rho_k^{(2)}\right) &= \text{Tr}\left((I \otimes Z^{(j_2)})(\rho_k^{(1)} \otimes \rho_k^{(2)})\right),\end{aligned}$$

where  $I$  is the identity operator. Therefore, we can relabel the qubit for the combined system described by the density operator  $\rho_k^{(1)} \otimes \rho_k^{(2)}$  as running from  $j = 1$  to  $j = n_1 + n_2$ . Using this notation, the above expectations can be re-expressed as

$$\begin{aligned}\text{Tr}\left(Z^{(j_1)}\rho_k^{(1)}\right) &= \text{Tr}\left(Z^{(j)}\rho_k^{(1)} \otimes \rho_k^{(2)}\right), \quad j = j_1 \\ \text{Tr}\left(Z^{(j_2)}\rho_k^{(2)}\right) &= \text{Tr}\left(Z^{(j)}\rho_k^{(1)} \otimes \rho_k^{(2)}\right), \quad j = n_1 + j_2.\end{aligned}$$

Following this idea, write out the outputs of two systems as follows,

$$\begin{aligned}\bar{y}_k^{(1)} &= C_1 + \sum_{d_1=1}^{R_1} \sum_{i_1=1}^{n_1} \cdots \sum_{i_{n_1}=i_{n_1-1}+1}^{n_1} \sum_{r_{i_1}+\cdots+r_{i_{n_1}}=d_1} w_{i_1, \dots, i_{n_1}}^{r_{i_1}, \dots, r_{i_{n_1}}} \langle Z^{(i_1)} \rangle_k^{r_{i_1}} \cdots \langle Z^{(i_{n_1})} \rangle_k^{r_{i_{n_1}}}, \\ \bar{y}_k^{(2)} &= C_2 + \sum_{d_2=1}^{R_2} \sum_{j_1=1}^{n_2} \cdots \sum_{j_{n_2}=j_{n_2-1}+1}^{n_2} \sum_{r_{j_1}+\cdots+r_{j_{n_2}}=d_2} w_{j_1, \dots, j_{n_2}}^{r_{j_1}, \dots, r_{j_{n_2}}} \langle Z^{(j_1)} \rangle_k^{r_{j_1}} \cdots \langle Z^{(j_{n_2})} \rangle_k^{r_{j_{n_2}}}.\end{aligned}$$

For any  $\lambda \in \mathbb{R}$ , let  $n = n_1 + n_2$  and  $k$  denotes the qubit index of the combined system running from  $k = 1$  to  $k = n$ , and  $R = \max\{R_1, R_2\}$ , then

$$\bar{y}_k^{(1)} + \lambda \bar{y}_k^{(2)} = C_1 + \lambda C_2 + \sum_{d=1}^R \sum_{k_1=1}^n \cdots \sum_{k_n=k_{n-1}+1}^n \sum_{r_{k_1}+\cdots+r_{k_n}=d} \bar{w}_{k_1, \dots, k_n}^{r_{k_1}, \dots, r_{k_n}} \langle Z^{(k_1)} \rangle_k^{r_{k_1}} \cdots \langle Z^{(k_n)} \rangle_k^{r_{k_n}},$$

where the weights  $\bar{w}_{k_1, \dots, k_n}^{r_{k_1}, \dots, r_{k_n}}$  are changed accordingly. For instance, if all  $k_m \leq n_1$ , then  $\bar{w}_{k_1, \dots, k_n}^{r_{k_1}, \dots, r_{k_n}} = w_{i_1, \dots, i_{n_1}}^{r_{i_1}, \dots, r_{i_{n_1}}}$ , corresponding to the weights for the output  $\bar{y}_k^{(1)}$ . Similarly, let  $R = R_1 + R_2$ ,

$$\bar{y}_k^{(1)} \bar{y}_k^{(2)} = C_1 C_2 + \sum_{d=1}^R \sum_{k_1=1}^n \cdots \sum_{k_n=k_{n-1}+1}^n \sum_{r_{k_1}+\cdots+r_{k_n}=d} \hat{w}_{k_1, \dots, k_n}^{r_{k_1}, \dots, r_{k_n}} \langle Z^{(k_1)} \rangle_k^{r_{k_1}} \cdots \langle Z^{(k_n)} \rangle_k^{r_{k_n}}.$$

Therefore,  $\bar{y}_k^{(1)} + \lambda \bar{y}_k^{(2)}$  and  $\bar{y}_k^{(1)} \bar{y}_k^{(2)}$  again have the same form as the right hand side of Eq. (3) in the main text. This implies that for any functionals  $F^{T^{(1)}}, F^{T^{(2)}} \in \mathcal{F}$ ,  $F^{T^{(1)}} + \lambda F^{T^{(2)}} \in \mathcal{F}$  and  $F^{T^{(1)}} F^{T^{(2)}} \in \mathcal{F}$ . Thus,  $\mathcal{F}$  forms a polynomial algebra.

It remains to show that  $T = T^{(1)} \otimes T^{(2)}$  is convergent, this will imply that  $F^{T^{(1)}} + \lambda F^{T^{(2)}}$  and  $F^{T^{(1)}} F^{T^{(2)}}$  are  $w$ -fading memory by Lemma 10, and that  $\mathcal{F}$  forms a polynomial algebra consisting of  $w$ -fading memory functionals. For all  $k \in \mathbb{Z}^+$ , consider  $T(u_k) = T^{(1)}(u_k) \otimes T^{(2)}(u_k)$ . Let  $\rho_{m*}$  be the unique fixed density operator of  $T^{(m)}(u_k)$ . Since  $T(u_k)$  only acts on separable states,  $\rho_* = \rho_{1*} \otimes \rho_{2*}$  is the unique fixed density operator of  $T(u_k)$ . Furthermore, adopting the proof of [18, Proposition 3], let  $A = \sum_i A_i \otimes \tilde{A}_i$  be a traceless Hermitian operator. Without loss of generality, we assume that  $\{\tilde{A}_i\}$  is an orthonormal set with respect to the Hilbert-Schmidt inner product. Then  $\{A_i \otimes \tilde{A}_i\}$  and  $\{T^{(1)}(u_k)|_{H_0} A_i \otimes \tilde{A}_i\}$  are orthogonal. By the Pythagoras theorem,  $T^{(1)}(u_k)|_{H_0} \otimes I$  on the hyperplane of traceless Hermitian operators satisfies

$$\begin{aligned} \|T^{(1)}(u_k)|_{H_0} \otimes I \sum_i A_i \otimes \tilde{A}_i\|^2 &= \sum_i \|T^{(1)}(u_k)|_{H_0} A_i \otimes \tilde{A}_i\|^2 = \sum_i \|T^{(1)}(u_k)|_{H_0} A_i\|^2 \|\tilde{A}_i\|^2 \\ &\leq \|T^{(1)}(u_k)|_{H_0}\|^2 \sum_i \|A_i\|^2 \|\tilde{A}_i\|^2 = \|T^{(1)}(u_k)|_{H_0}\|^2 \|\sum_i A_i \otimes \tilde{A}_i\|^2. \end{aligned}$$

Thus,  $\|T^{(1)}(u_k)|_{H_0} \otimes I\| \leq \|T^{(1)}(u_k)|_{H_0}\|$ . Similarly, a symmetric argument shows that  $\|I \otimes T^{(2)}(u_k)|_{H_0}\| < \|T^{(2)}(u_k)|_{H_0}\|$ . Therefore, when restricted to traceless Hermitian operators,

$$\begin{aligned} \|(T^{(1)}(u_k) \otimes T^{(2)}(u_k))|_{H_0}\| &= \|(T^{(1)}(u_k)|_{H_0} \otimes I)(I \otimes T^{(2)}(u_k)|_{H_0})\| \\ &\leq \|T^{(1)}(u_k)|_{H_0} \otimes I\| \|I \otimes T^{(2)}(u_k)|_{H_0}\| \leq \|T^{(1)}(u_k)|_{H_0}\| \|T^{(2)}(u_k)|_{H_0}\| \\ &< (1 - \epsilon)^2 < 1 - \epsilon. \end{aligned}$$

The convergence of  $T$  follows from Theorem 4.  $\square$

#### D. A universal class

We now prove the universality of the class of dissipative quantum systems introduced in the main text. Recall that this class consists of  $N$  non-interacting quantum sub-systems, where the dynamics of subsystem  $K$  with  $n_K$  qubits is governed by the CPTP map:

$$T_K(u_k) \rho_{k-1}^K = \text{Tr}_{i_0^K} (e^{iH_K \tau} \rho_{k-1}^K \otimes \rho_{i_0, k}^K e^{-iH_k \tau}), \quad (8)$$

where

$$\rho_{i_0, k}^K = u_k |0\rangle\langle 0| + (1 - u_k) |1\rangle\langle 1|, \quad 0 \leq u_k \leq 1$$

$$H_K = \sum_{j_1=0}^{n_K} \sum_{j_2=j_1+1}^{n_K} J_K^{j_1, j_2} (X^{(i_{j_1}^K)} X^{(i_{j_2}^K)} + Y^{(i_{j_1}^K)} Y^{(i_{j_2}^K)}) + \sum_{j=0}^{n_K} \alpha Z^{(i_j^K)}, \quad (9)$$

with  $J_K^{j_1, j_2}$  and  $\alpha$  are real-valued constants and  $\text{Tr}_{i_0^K}$  denotes the partial trace over the ancilla qubit. Let  $\overline{H}_K = I \otimes \cdots \otimes H_K \otimes \cdots \otimes I$  with  $H_K$  in the  $K$ -th position, the total Hamiltonian of  $N$  sub-systems is

$$H = \sum_{K=1}^N \overline{H}_K. \quad (10)$$

Writing  $\rho_k = \otimes_{K=1}^N \rho_k^K$ , the overall dynamics and the output are given by

$$\begin{cases} \rho_k = T(u_k)\rho_{k-1} = \otimes_{K=1}^N T_K(u_k)\rho_{k-1}^K \\ \bar{y}_k = h(\rho_k), \end{cases} \quad (11)$$

where  $h$  is the multivariate polynomial defined by the right hand side of Eq. (3) in the main text.

**Proposition 13.** *Let  $\mathcal{M}_S$  be the set of filters induced from dissipative quantum systems described by Eq. (11) such that each  $T_K$  ( $K = 1, \dots, N$ ) satisfies conditions in Theorem 4. Then for any null sequence  $w$ , the corresponding family of functionals  $\mathcal{F}_S$  is dense in  $C(K_1^-[0, 1], \|\cdot\|_w)$ .*

*Proof.* We first show  $T_K(x)$  is continuous in the operator norm with respect to  $x$  for all  $x \in [0, 1]$ . Let  $x, y \in [0, 1]$  and  $Z$  be the Pauli  $Z$  operator. By the definition of induced operator norm,

$$\begin{aligned} \|T_K(x) - T_K(y)\| &= \sup_{\substack{A \in \mathcal{L}(\mathbb{C}^{2^n}) \\ \|A\|=1}} \|(T_K(x) - T_K(y))A\| \\ &= \sup_{\substack{A \in \mathcal{L}(\mathbb{C}^{2^n}) \\ \|A\|=1}} \|\text{Tr}_{i_0}^K(e^{iH_K\tau} A \otimes (x - y)Z e^{-iH_K\tau})\| \\ &= |x - y| \sup_{\substack{A \in \mathcal{L}(\mathbb{C}^{2^n}) \\ \|A\|=1}} \|\text{Tr}_{i_0}^K(e^{iH_K\tau} A \otimes Z e^{-iH_K\tau})\| \\ &= |x - y| \|\tilde{T}\|, \end{aligned}$$

where  $\tilde{T}$  is an input-independent CPTP map. We therefore have established the continuity condition for  $T_K(x)$ .

Now, the same argument in the proof of Lemma 12 shows that  $T = T_1 \otimes \dots \otimes T_N$  is convergent given the assumptions on each  $T_K$ . Furthermore, given two convergent systems whose dynamics are described by Eq. (11) with Hamiltonians  $H^{(1)}$  and  $H^{(2)}$ , the total Hamiltonian of the combined system is  $H = H^{(1)} \otimes I + I \otimes H^{(2)}$ , which again has the form Eq. (10). Therefore, by the above observation and Lemma 12,  $\mathcal{F}_S$  forms a polynomial algebra, consisting of  $w$ -fading memory functionals for any null sequence  $w$ .

It remains to show  $\mathcal{F}_S$  contains constants and separates points. Constants can be obtained by setting all weights in the output to be zero. To show the family  $\mathcal{F}_S$  separates points, we state the following lemma for later use, whose proof can be found in [19, Theorem 3.2].

**Lemma 14.** *Let  $f(\theta) = \sum_{n=0}^{\infty} x_n \theta^n$  be a non-constant real power series, having a non-zero radius of convergence. If  $f(0) = 0$ , then there exists  $\beta > 0$  such that  $f(\theta) \neq 0$  for all  $\theta$  with  $|\theta| \leq \beta$  and  $\theta \neq 0$ .*

Consider a single-qubit system interacting with a single ancilla qubit whose dynamics is governed by Eq. (11). Order an orthogonal basis of  $\mathcal{L}(\mathbb{C}^2)$  as  $\mathcal{B} = \{I, Z, X, Y\}$ . Recall that the normal representation of a CPTP map  $T$  and a density operator  $\rho$  are given by

$$\overline{T}_{i,j} = \frac{\text{Tr}(B_i T(B_j))}{2} \quad \text{and} \quad \overline{\rho}_i = \frac{\text{Tr}(\rho B_i)}{2},$$

where  $B_i \in \mathcal{B}$ . Without loss of generality, let  $\tau = 1$  and set  $J_1^{j_1, j_2} = J \in \mathbb{R}$  for all  $j_1, j_2$  in the Hamiltonian given by Eq. (9). We obtain the normal representation of the CPTP map defined in Eq. (8) as follows

$$\overline{T}(u_k) = \begin{pmatrix} 1 & 0 & 0 & 0 \\ \sin^2(2J)(2u_k - 1) & \cos^2(2J) & 0 & 0 \\ 0 & 0 & \cos(2J)\cos(2\alpha) & \cos(2J)\sin(2\alpha) \\ 0 & 0 & -\cos(2J)\sin(2\alpha) & \cos(2J)\cos(2\alpha) \end{pmatrix}.$$

The eigenvalues are independent of input  $u_k$ :

$$\lambda_1 = e^{i2\alpha} \cos(2J), \lambda_2 = e^{-i2\alpha} \cos(2J), \lambda_3 = \cos^2(2J), \lambda_4 = 1.$$

Choose  $J \neq \frac{z\pi}{2}$  for  $z \in \mathbb{Z}$  such that  $|\cos(2J)| < 1 - \epsilon$  and  $\cos^2(2J) < (1 - \epsilon)^2$  for some  $\epsilon > 0$ . Then  $\lambda_4 = 1$  is simple and is the unique eigenvalue with  $|\lambda| = 1$ . Furthermore, the map restricted to the hyperplane of traceless Hermitian operators is

$$\overline{T}|_{H_0} = \begin{pmatrix} \cos^2(2J) & 0 & 0 \\ 0 & \cos(2J)\cos(2\alpha) & \cos(2J)\sin(2\alpha) \\ 0 & -\cos(2J)\sin(2\alpha) & \cos(2J)\cos(2\alpha) \end{pmatrix}$$

with  $\|\overline{T}|_{H_0}\| = |\cos(2J)|$ . By Theorem 4,  $T$  is convergent and we choose an arbitrary initial density operator  $\overline{\rho}_{-\infty} = (1 \ 1 \ 0 \ 0)^T$ . If we only take the expectation  $\langle Z \rangle$ , then the multivariate polynomial output given by Eq. (3) in the main text induces the functional

$$F^T(u) = w \left[ \overrightarrow{\prod}_{j=0}^{\infty} \overline{T}(u_{-j}) \overline{\rho}_{-\infty} \right]_2 + C,$$

where  $[\cdot]_2$  refers to the second element of the vector, corresponding to  $\langle Z \rangle$  given the order of the orthogonal basis  $\mathcal{B}$ . Given two input sequences  $u \neq v$ , consider two cases:

(i) If  $u_0 \neq v_0$ , choose  $J = \frac{\pi}{4}$  such that  $\cos^2(2J) = 0$ . Then

$$F^T(u) - F^T(v) = w(2u_0 - 2v_0) \neq 0.$$

(ii) If  $u_0 = v_0$ ,

$$F^T(u) - F^T(v) = 2w \sin^2(2J) \sum_{j=0}^{\infty} (\cos^2(2J))^j (u_{-j} - v_{-j}).$$

Let  $\theta = \cos^2(2J)$ , then given our choice of  $J$ ,  $0 \leq \theta < 1 - \epsilon$  and  $\sin^2(2J) > \epsilon$ . Consider the power series

$$f(\theta) = \sum_{j=0}^{\infty} \theta^j (u_{-j} - v_{-j}),$$

since  $|u_{-j} - v_{-j}| \leq 1$ ,  $f(\theta)$  has a non-zero radius of convergence  $R$  such that  $(-1, 1) \subseteq R$ . Moreover,  $f(\theta)$  is non-constant and  $f(0) = 0$ . The separation of points follows from invoking Lemma 14.

Finally, the universality property of  $\mathcal{F}_S$  follows from Theorem 9.  $\square$

## E. Detailed experimental settings

In this section, we describe detailed formulas for the NARMA tasks, simulation of decoherence and experimental conditions for ESNs and the Volterra series.

### 1. The NARMA task

The general  $m$ th-order NARMA I/O map is described as [3]:

$$y_k = 0.3y_{k-1} + 0.05y_{k-1} \left( \sum_{j=0}^{\tau_{\text{NARMA}}-1} y_{k-j-1} \right) + 1.5u_{k-\tau_{\text{NARMA}}}u_k + \gamma.$$

where  $\gamma \in \mathbb{R}$ . In the main text, we consider  $\tau_{\text{NARMA}} = \{15, 20, 30, 40\}$ . For  $\tau_{\text{NARMA}} = \{15, 20\}$ , we set  $\gamma = 0.1$ . For  $\tau_{\text{NARMA}} = \{30, 40\}$ ,  $\gamma$  is set to be 0.05 and 0.04 respectively. A randomly generated input sequence in the range  $[0, 0.2]$  is deployed for all the NARMA tasks. This range is chosen to ensure convergence of the NARMA tasks.

### 2. Decoherence

We consider dephasing and decaying noise, which are of experimental importance. To employ the dephasing noise, we implement single-qubit phase-flip for all  $n + 1$  qubits, including the  $n$  system qubits and the ancilla qubit. That is for  $j = 1, \dots, n + 1$  the system density operator undergoes:

$$\rho \rightarrow \frac{1 + e^{-2\gamma S\tau}}{2} \rho + \frac{1 - e^{-2\gamma S\tau}}{2} Z^{(j)} \rho Z^{(j)},$$

where  $Z^{(j)}$  denotes the Pauli  $Z$  for qubit  $j$ . To deploy the decaying noise, all  $n + 1$  qubits undergo the amplitude damping channel whose Kraus operators are given by

$$M_0 = \begin{pmatrix} 1 & 0 \\ 0 & \sqrt{\frac{1-e^{-2\gamma S\tau}}{2}} \end{pmatrix}, M_1 = \begin{pmatrix} 0 & \sqrt{\frac{1+e^{-2\gamma S\tau}}{2}} \\ 0 & 0 \end{pmatrix}.$$

For  $j = 1, \dots, n + 1$ , the system density operator thus evolves as

$$\rho \rightarrow M_0^{(j)} \rho (M_0^{(j)})^\dagger + M_1^{(j)} \rho (M_1^{(j)})^\dagger,$$

where  $M_l^{(j)}$  ( $l = 0, 1$ ) is the Kraus operator  $M_l$  for qubit  $j$  and  $(M_l^{(j)})^\dagger$  denotes the adjoint of  $M_l^{(j)}$ . In the numerical experiments, we consider  $\gamma/S = \{10^{-1}, 10^{-2}, 10^{-3}\}$  which are within the experimentally feasible range for systems like NMR ensembles [36].

Following the discussion in Sec. V B, Fig. 8 plots the average sum of modulus of off-diagonal elements in the density operator, for the last 50 timesteps of the NARMA20 validation series.

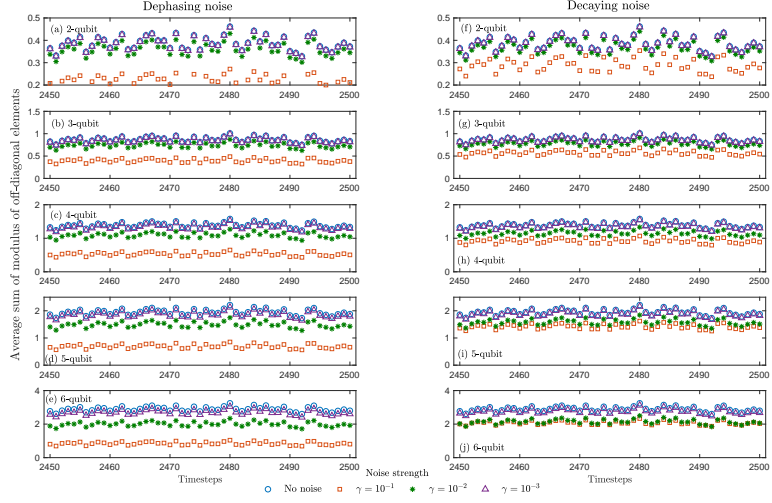


FIG. 8. Average sum of modulus of off-diagonal elements in the density operator, for the last 50 timesteps of the NARMA20 validation sequence

### 3. The echo state networks

An ESN with  $m$  nodes is a type of recurrent neural network with a  $m \times 1$  input matrix  $W_i$ , a  $m \times m$  reservoir matrix  $W_r$  and an  $1 \times m$  output matrix  $W_o$ . The state evolution and output are given by [16]

$$\begin{cases} x_k = \tanh(W_r x_{k-1} + W_i u_k) \\ \hat{y}_k = W_o x_k, \end{cases}$$

where  $\tanh(\cdot)$  is an element-wise operation.

In the numerical examples, lengths of washout, learning and evaluation phases for ESNs and SA are the same. Given an output sequence  $y$  to be learned, the output weights  $W_o$  are optimized via linear least squares to minimize the mean-squared error  $\sum_k |y_k - \hat{y}_k|^2$  in the training phase. We now detail the experimental conditions for ESNs in various subsections of the numerical experiments (Sec. V) in the main text.

For the comparison given in Subsection V A, we set the reservoir size to be  $\{10, 20, 30, 40, 50, 100, 150, 200, 250, 300, 400, 500, 600, 700, 800\}$ . The number of computational nodes is the same as the reservoir size (state-space size) of the ESNs in this experiment. The results for ESNs are reported as the average NMSE for all the NARMA tasks. The average NMSE for ESNs is obtained as follows. For each reservoir size, we prepare 100 ESNs with elements of  $W_r$  randomly generated from the range  $[-2, 2]$ . For each of these ESNs, we select the spectral radius to be 20 values evenly spaced between  $[0.01, 0.99]$  to ensure convergence. For each of the chosen spectral radius, the elements of  $W_i$  are randomly chosen within  $[-\delta, \delta]$ , where  $\delta$  is set to be  $\{0.01, 0.1, 0.5, 1\}$ . As an example, for reservoir size 10, spectral radius 0.99 and  $\delta = 1$ , 100 ESNs are generated by randomly choosing elements of  $W_r$  from  $[-2, 2]$ . To obtain the average ESNs NMSE as the reservoir size varies, we average over the spectral radius and  $\delta$ . Table 2 and Fig. 9 summarize the average ESNs NMSE for the NARMA15 and NARMA20 tasks.

For the further comparison provided in Subsection V D, ESNs are simulated to approxi-

Reservoir size	NARMA15		NARMA20	
	Average NMSE	Standard error	Average NMSE	Standard error
	$(\times 10^{-3})$	$(\times 10^{-3})$	$(\times 10^{-3})$	$(\times 10^{-3})$
10	3.4	0.023	4.0	0.046
20	3.2	0.048	4.0	0.063
30	3.0	0.038	3.9	0.065
40	2.9	0.032	3.8	0.055
50	2.8	0.045	3.7	0.049
100	2.6	0.062	3.6	0.029
150	2.5	0.038	3.5	0.025
200	2.4	0.029	3.4	0.034
250	2.3	0.021	3.4	0.046
300	2.3	0.021	3.3	0.041
400	2.2	0.014	3.3	0.042
500	2.2	0.012	3.3	0.038
600	2.2	0.014	3.2	0.028
700	2.1	0.017	3.2	0.027
800	2.1	0.016	3.2	0.029

TABLE 2. Average ESNs NMSE for NARMA15 and NARMA20 tasks. Results are rounded to two significant figures.

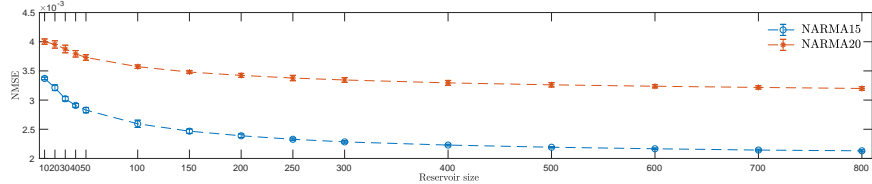


FIG. 9. Average NMSE of ESNs for NARMA15 and NARMA20. The error bars represent the standard error

mate NARMA15, NARMA20, NARMA30 and NARMA40. The reservoir size of ESNs for each learning task is set to be  $\{496, 600, 700, 800\}$ . The number of computational nodes for ESNs is set to be

$$C_4 \cup C_5 \cup C_6 = \{4, 5, 6, 14, 20, 27, 34, 55, 69, 83, 125, 209, 251, 329, 461, 494\},$$

where  $C_n$  denotes the chosen numbers of computational nodes for  $n$ -qubit SA defined as follows. Recall that in this experiment, 4-, 5- and 6-qubit SA with varying degrees  $R$  in the output are chosen. For 4-qubit SA,  $R = \{1, \dots, 8\}$  correspond to the number of computational nodes  $C_4 = \{4, 14, 34, 69, 125, 209, 329, 494\}$ . For 5-qubit SA,  $R = \{1, \dots, 6\}$ , such that  $C_5 = \{5, 20, 55, 125, 251, 461, 461, 461\}$ . For 6-qubit SA,  $R = \{1, \dots, 5\}$ , such that  $C_6 = \{6, 27, 83, 209, 461, 461, 461, 461\}$ .

For each reservoir size and each number of computational nodes for ESNs, we prepare 100 ESNs with elements of  $W_r$  randomly generated from the range  $[-2, 2]$ . For each of these ESNs, the spectral radius is set to be 20 values evenly spaced between  $[0.01, 0.99]$ . For each of the chosen spectral radius, the elements of  $W_i$  are randomly chosen within  $[-\delta, \delta]$ , where  $\delta$  is set to be 20 values evenly spaced between  $[0.01, 1]$ . As an example, for reservoir size 496, 4 computational nodes, spectral radius 0.99 and  $\delta = 1$ , 100 ESNs are randomly generated by randomly choosing elements  $W_r$  from  $[-2, 2]$ . To obtain the average ESN NMSE as the reservoir size and number of computational nodes vary, we average over the spectral radius and  $\delta$ . These averaged results are summarized in Fig. 7 in Sec. V D.

#### 4. The Volterra series

The discrete finite Volterra series with kernel order  $k$  and memory  $p$  is given by [6]

$$\hat{y}_k = h_0 + \sum_{i=1}^k \sum_{j_1, \dots, j_i=0}^{p-1} h_i^{j_1, \dots, j_i} \prod_{l=1}^i u_{k-j_l},$$

where  $u_{k-j}$  is the delayed input,  $h_0$  is a real-valued constant, and  $h_i^j$  are real-valued kernel coefficients (or output weights in our context). Notice that when memory  $p = 1$ , the Volterra series is a map from the current input  $u_k$  to the output  $\hat{y}_k$ . The kernel coefficients are optimized via linear least squares to minimize the mean-squared error  $\sum_k |y_k - \hat{y}_k|^2$  in the learning phase, where  $y$  is the target output sequence to be learned.

The number of computational nodes, that is the number of kernel coefficients  $h_i^j$ , is given by  $(p^{k+1} - p)/(p - 1)$ . We vary the parameters of the Volterra series as follows: for each  $k = \{2, \dots, 8\}$ , choose  $p$  from  $\{2, \dots, 27\}$  such that the maximum number of computational nodes does not exceed 800. For any value of  $k$  and  $p$  beyond their respective ranges, the number of computational nodes will exceed 800. Note that for  $k = 1$ , the output of the Volterra series is a linear function of delayed inputs. Since we are interested in nonlinear I/O maps, we choose  $k \geq 2$ . Table 3 summarizes the corresponding number of computational nodes as  $k$  and  $p$  vary. Fig. 10 shows the Volterra series NMSE according to the kernel order and memory.

$k \backslash p$	2	3	4	5	6	7	8	9	10	11	12	13	14	15	16	17	18	19	20	21	22	23	24	25	26	27
2	6	12	20	30	42	56	72	90	110	132	156	182	210	240	272	306	342	380	420	462	506	552	600	650	702	756
3	14	39	84	155	258	399	584																			
4	30	120	340	780																						
5	62	363																								
6	126																									
7	254																									
8	510																									

TABLE 3. Values of  $k$  and  $p$  for the Volterra series and the corresponding number of computational nodes. The empty entries indicate that for the chosen  $k$  and  $p$ , the number of computational nodes exceeds 800

It is observed in Fig. 10 that as the kernel order increases, the Volterra series task performance does not improve. On the other hand, as the memory increases for kernel order 2, the Volterra series task performance improves. The improvement is particularly significant as the memory  $p$  coincides with the delay for the NARMA task, that is  $p = \tau_{\text{NARMA}} + 1$ . For instance, when kernel order is 2, as the memory increases beyond 16 for the Volterra series, the NMSE decreases from  $4 \times 10^{-3}$  to less than  $10^{-3}$  for NARMA15. Similarly, as the memory increases beyond 21, the NMSE decreases from  $5 \times 10^{-3}$  to approximately  $2 \times 10^{-3}$ .

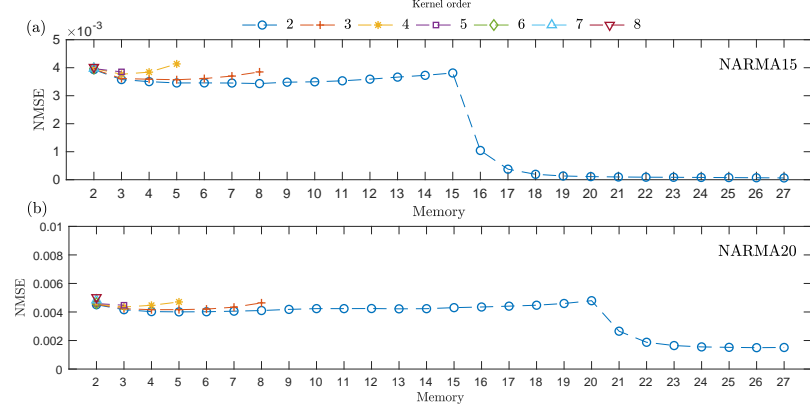


FIG. 10. NMSE of the Volterra series according to kernel order and memory. (a) shows the Volterra series NMSE for NARMA15 and (b) shows the Volterra series NMSE for NARMA20

---

[1] Aaronson, S. and Arkhipov, A., in *Proceedings of the 43rd ACM Symposium on Theory of Computing (STOC)* (2011) pp. 333–342.

[2] Appelant, L. *et al.*, *Nat. Commun.* **2**, 468 (2011).

[3] Atiya, A. F. and Parlos, A. G., *IEEE Trans. Neural Netw.* **11**, 697 (2000).

[4] Boixo, S., Isakov, S. V., Smelyanskiy, V. N., Babbush, R., Ding, N., Jiang, Z., Bremner, M. J., Martinis, J. M., and Neven, H., “Characterizing quantum supremacy in near-term devices,” (2017), arXiv preprint. [Online] Available: <https://arxiv.org/abs/1608.00263>.

[5] Boutsen, L., van Handel, R., and James, M. R., *SIAM Rev.* **51**, 239 (2009).

[6] Boyd, S. and Chua, L., *IEEE Trans. Circuits Syst.* **32**, 1150 (1985).

[7] Bremner, M. J., Jozsa, R., and Shepherd, D. J., *Proc. Royal Soc. A* **467**, 459 (2010).

[8] Buehner, M. and Young, P., *IEEE Trans. Neural Netw.* **17**, 820 (2006).

[9] Burgarth, D. and Giovannetti, V., *New Journal of Physics* **9**, 150 (2007).

[10] Dieudonné, J., *Foundations of Modern Analysis* (Read Books Ltd, 2013).

[11] Farhi, E., Goldstone, J., and Gutmann, S., “A quantum approximate optimization algorithm,” (2014), arXiv preprint. [Online] Available: <https://arxiv.org/abs/1411.4028>.

[12] Fujii, K. and Nakajima, K., *Phys. Rev. Appl.* **8**, 024030 (2017).

[13] Grigoryeva, L. and Ortega, J., “Echo state networks are universal,” (2018), arXiv preprint. [Online] Available: <https://arxiv.org/abs/1806.00797>.

[14] Grigoryeva, L. and Ortega, J., “Universal discrete-time reservoir computers with stochastic inputs and linear readouts using non-homogeneous state-affine systems,” (2018), arXiv preprint. [Online] Available: <https://arxiv.org/abs/1712.00754>.

[15] Gross, J. A., Caves, C. M., Milburn, G. J., and Combes, J., *Quantum Science and Technology* **3**, 024005 (2018).

[16] Jaeger, H. and Haas, H., *Science* **304**, 5667 (2004).

[17] Kandala, A., Mezzacapo, A., Temme, K., Takita, M., Brink, M., Chow, J. M., and Gambetta, J. M., *Nature* **549**, 242 (2017).

[18] Kubrusly, C. S., *Far East Journal of Mathematical Sciences* **22**, 137 (2006).

[19] Lang, S., *Complex Analysis*, Graduate Texts in Mathematics (Springer-Verlag, 1985).

[20] Le Gall, F., in *Foundations of Computer Science (FOCS), 2012 IEEE 53rd Annual Symposium on* (IEEE, 2012) pp. 514–523.

[21] Lukoševičius, M., in *Neural networks: Tricks of the trade* (Springer, 2012) pp. 659–686.

[22] Lukoševičius, M. and Jaeger, H., *Computer Science Review* **3**, 127 (2009).

[23] Lund, A. P., Bremner, M. J., and Ralph, T. C., *npj Quantum Information* **3**, 15 (2017).

[24] Maass, W., Natschläger, T., and Markram, H., *Neural Computation* **14**, 2531 (2002).

[25] McClean, J. R., Romero, J., Babbush, R., and Aspuru-Guzik, A., *New J. Phys.* **18** (2016).

[26] Mills, M., *IEEE Annals of the History of Computing* **22**, 24 (2011).

[27] Mitarai, K., Negoro, M., Kitagawa, M., and Fujii, K., “Quantum circuit learning,” (2018), arXiv preprint. [Online] Available: <https://arxiv.org/abs/1803.00745>.

[28] Nakajima, K. *et al.*, “Boosting computational power through spatial multiplexing in quantum reservoir computing,” (2018), arXiv preprint. [Online] Available: <https://arxiv.org/abs/1803.04574>.

[29] Otterbach, J. S. *et al.*, “Unsupervised machine learning on a hybrid quantum computer,” (2017), arXiv preprint. [Online] Available: <https://arxiv.org/abs/1712.05771>.

[30] Pavlov, A., van de Wouw, N., and Nijmeijer, H., in *Control and Observer Design for Nonlinear Finite and Infinite Dimensional Systems*, Lecture Notes in Control and Information Science, Vol. 322, edited by T. Meurer, K. Graichen, and E. D. Gilles (Springer, 2005) pp. 131–146.

[31] Perez-Garcia, D., Wolf, M. M., Petz, D., and Ruskai, M. B., *Journal of Mathematical Physics* **47**, 083506 (2006).

[32] Peruzzo, A., McLean, J., Shadbolt, P., Yung, M., Zhou, X., Love, P. J., Aspuru-Guzik, A., and O’Brien, J. L., *Nature Comms* **5** (2013).

[33] Preskill, J., “Quantum computing in the NISQ era and beyond,” (2018), arxiv preprint, [Online] Available: <https://arxiv.org/abs/1801.00862>.

[34] Richter, S. and Werner, R. F., *Journal of Statistical Physics* **82**, 963 (1996).

[35] Torrejon, J. *et al.*, *Nature* **547**, 428 (2017).

[36] Vandersypen, L. M., Steffen, M., Breyta, G., Yannoni, C. S., Sherwood, M. H., and Chuang, I. L., *Nature* **414**, 883 (2001).

[37] Wang, D., Higgott, O., and Brierley, S., “A generalised variational quantum eigensolver,” (2018), arXiv preprint. [Online] Available: <https://arxiv.org/abs/1802.00171>.